A modal approach for the identification of joint and link compliance of an industrial manipulator

Michele Tonan[1], Matteo Bottin[1], Alberto Doria[1] and Giulio Rosati[1]

[1] University of Padova, Italy
michele.tonan@phd.unipd.it
matteo.bottin@unipd.it
alberto.doria@unipd.it
giulio.rosati@unipd.it

Abstract. A method for the identification of joint stiffness making use of modal tests carried out in specific robot configurations is presented. The experimental results show the presence of a resonance peak related to structural compliance as well. Therefore, a method for the identification of the structural compliance based on the Mozzi's axis theorem is presented. This method makes it possible to define a compliance axis that models the effect of structural compliance.

Keywords: Industrial robots, Compliance, Mozzi's axis, Modes of vibration.

1 Introduction

In the last years, industrial robots have been widely used for applications in which the structure of the robot is excited either by high external loads or by high dynamic forces. In such applications, the compliance of both the joints and the links of the robot is not negligible [1]. This aspect may result in poor robot performance, which is directly correlated to higher production costs. Then, it is crucial to properly identify joint and link compliances to better calculate the real robot capabilities, or it is crucial to increase structural stiffness [2]. Several authors have studied joint and link stiffness, and many approaches have been proposed. Some of them rely on the measurement of the end effector position, either via optical and laser systems [3, 5] or via closed chain fixtures [6]. As a result, such methods are not applicable to all industrial applications due to high equipment costs or encumbrance. In this paper, the modal approach proposed in [7] is extended to identify the stiffness of the first three joints of an industrial robot and the compliance of the first link. Moreover, the Mozzi's axis concept [8, 9] is used to find the compliance axis of the first link. The paper is structured as follows: sections 2-3 describe the experimental setup and joint compliance; section 4 describes the mathematical model of the Mozzi's axis, which is used in section 5 for the identification of the compliance axis of the link; conclusions are drawn in section 6.

2 Configurations to identify the joints compliance

In this paper the same approach of [7] is applied to a new robot Mitsubishi RV4-FRL to identify the stiffness of the first three joints. To perform the modal tests eighteen test points were chosen. Figure 1 shows the robot and the test points. In Table 1 the Denavit Hartenberg (DH) parameters of the transformation matrices from link i to j are reported [10].

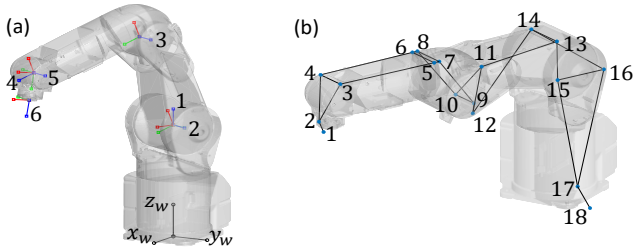

Fig. 1. Robot Mitsubishi RV4-FRL. (a) DH frames of this robot (red line represents X axis; green line represents Y axis; blue line represents Z axis). (b) Robot with test points.

Table 1. Denavit Hartenberg parameters of robot Mitsubishi RV4-FRL.

$T_{i,j}$	α_{i-1} [°]	$a_{i-1}[m]$	θ_i[°]	$d_i[m]$	$T_{i,j}$	α_{i-1} [°]	$a_{i-1}[m]$	θ_i[°]	$d_i[m]$
1w	0	0	θ_1	0.350	**43**	-90	0.050	θ_4	0.335
21	-90	0	$\theta_2 - 90$	0	**54**	90	0	θ_5	0
32	0	0.350	$\theta_3 - 90$	0	**65**	-90	0	θ_6	0.085

In this analysis the robot links are assumed infinitely rigid whereas the joints cause the compliance of the robot. The vibration modes of a robot typically involve the rotations of some joints, and the natural frequencies are functions of the stiffness of these joints. Therefore, the main problem of modal methods for identifying joint stiffness is finding robot configurations with modes of vibrations dominated by the stiffness of only one joint. In this case, the modal stiffness coincides with the joint stiffness, and the latter can be identified from the measured natural frequency and the calculated value of the moment of inertia. Another important factor is the choice of appropriate excitation directions for the selected configurations. In this analysis the robot configurations were chosen to minimize the off-diagonal elements of the mass matrix to decouple as much as possible the joint of interest from the others. In Table 2 the joint angles of the test configurations are presented.

Table 2. Joint angles - robot test configurations.

Configuration	θ_1[°]	θ_2[°]	θ_3[°]	θ_4[°]	θ_5[°]	θ_6[°]
Test 1	-25	90	0	0	90	0
Test 2	-25	0	98	0	-9	0
Test 3	-25	-80	155	2	-75	0

Test configuration 1 was chosen to selectively excite joint 1. The robot is fully extended horizontally, to achieve the maximum excitation on joint 1 when a lateral impulse is applied. Test configuration 2 minimizes the excitation of joint 3 and maximizes the excitation of joint 2. Link 2 is vertical and the impulse force is applied along a line (perpendicular to the flange) that crosses the axis of joint 3. Actually, there is always an inertial cross-coupling between joints 2 and 3. This phenomenon chiefly affects the identification of joint 3 stiffness [7], since the inertial cross-coupling term is always small with respect the direct inertia of joint 2, but in some configurations, it may be comparable with the direct inertia of joint 3. Test configuration 3 is adopted to identify the stiffness of joint 3. Since the folded configuration minimizes the inertial cross-coupling term and the vertical force strongly excites joint 3 and has a small moment about joint 2. In Figure 2 the three configurations and the relative impulsive forces are shown.

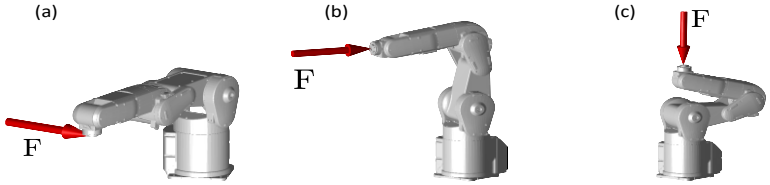

Fig. 2. Robot configurations and excitation forces. (a) Test 1. (b) Test 2. (c) Test 3.

3 Identification of joint compliance

Experimental tests were carried out using a PCB 086C01 hammer (sensitivity 0.25 mV/N) to excite the system, a PCB 356A17 tri-axial accelerometer (sensitivity 50 mV/(m/s^2)) and a data acquisition board NI9234. For each configuration the FRFs were acquired using a sampling rate of 1652 Hz and 2048 samples. The tests were carried out using the rowing response approach, the accelerometer was moved to 18 points, whereas the excitation was always applied to point 1. The natural frequencies dominated by the compliance of each joint were identified from the measured FRFs by means of the software ModalVIEW, they are reported in Table 3 together with the damping ratios. In Figure 3a all the FRFs obtained in test configuration 1 are reported. In this case, the natural frequency of joint 1 is equal to 14.8 Hz and the damping ratio is equal to 3.4%. In Figure 3b the sums of FRFs of points 1-14 and of points 15-18 are shown. This plot shows the presence of a large resonance peak at 14.8 Hz in all the FRFs of points 1-14. This result confirms that the mode at 14.8 Hz chiefly involves the first joint, because the points 1-14 are after this joint.

Table 3. Natural frequencies and damping ratios for first three joints.

	Joint 1	*Joint 2*	*Joint 3*
f [Hz]	14.8	19.2	38.8
ζ [%]	3.4	2.1	3.4

When the selected mode is dominated by the compliance of only one joint it is possible to evaluate the joint stiffness and the damping coefficient from the modal equation [7]:

$$k_i = \left(2\pi f_{n_i}\right)^2 I_{zz_i}(\boldsymbol{q_i}) \tag{1}$$

$$c_i = \frac{\zeta_i k_i}{\pi f_{ni}} \tag{2}$$

In which $i = 1 \ldots n$ (n is the number of joints) and $I_{zz_i}(\boldsymbol{q_i})$ is the moment of inertia about joint i in the selected configuration ($\boldsymbol{q_i}$). The calculated results are summarized in Table 4.

Table 4. Joint stiffness and damping.

	Joint 1	*Joint 2*	*Joint 3*
Stiffness [Nm/rad]	20789	24307	21243
Damping [Nms/rad]	15.2	8.6	5.9

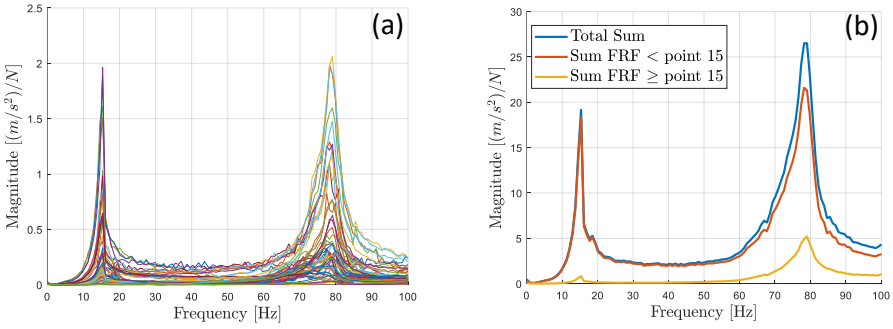

Fig. 3. FRFs between applied force and measured accelerations in configuration test 1. (a) Magnitude of all FRFs. (b) Total sum of FRFs magnitudes and sum of magnitudes of the FRFs before and after point 15.

Figure 3a clearly shows the presence of a tall resonance peak at 79 Hz with a damping ratio $\zeta = 2.6\%$. The mode shape at this specific frequency shows that this mode is not characteristic of a joint (or groups of joints), but it involves the structural deformation of the system. To corroborate the previous statement, a graphical representation of the displacements of the test points at 79 Hz is reported in Figure 4. From this figure is clear that there are relevant displacements in the X and Z direction, whereas the displacement in the Y direction is negligible. Displacements in the X direction are parallel to the axes of joints 2 and 3 and cannot be associated to a rigid rotation about joint 1. This behavior of the system suggests the presence of a structural compliance about an axis passing through link 1. This compliance can be caused by the flexion of the fork supporting link 2 or by the compliance of the bearing of joint 1. It is worth noticing that in the Figure 4b the first two measurement points are in phase opposition with respect to the other points and points 3 and 4 have small displacements: this phenomenon could be justified by a sloping position of the compliance axis that passes through link 1 and

near points 3 and 4. To evaluate the structural stiffness, first, the compliance axis related to the natural frequency of 79 Hz has to be calculated. Then, the inertia about this axis can be calculated from the CAD model of the robot and the stiffness value can be calculated by means Eq. (1).

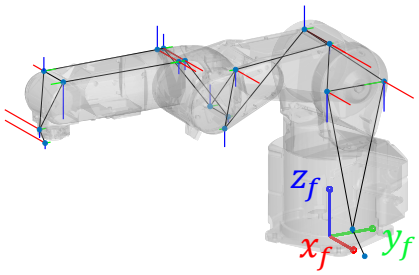

Fig. 4. Displacements of the test points at 79 Hz expressed in the fixed reference frame f.

4 Compliance axis

A method, based on the Mozzi's axis theorem, is proposed to evaluate the position of the compliance axis of link 1. This method is novel, since in a previous research [9] the Mozzi's axis theorem was used for representing the effect of joint compliance. A group of 3 points located in the stiff part of the robot arm is selected. They are assumed to move as a rigid body and define a rigid reference plane. Hence, the Mozzi's axis theorem can be applied and the motion of the reference plane can be described as a combination of a rotation about the Mozzi's axis and a translation along this axis. The general equation for studying the rigid motion of the reference plane is defined as:

$$\begin{Bmatrix} \dot{x}_P \\ \dot{y}_P \\ \dot{z}_P \end{Bmatrix}^f = \begin{Bmatrix} \dot{x}_Q \\ \dot{y}_Q \\ \dot{z}_Q \end{Bmatrix}^f + [R]_m^f \begin{bmatrix} 0 & -\omega_z & \omega_y \\ \omega_z & 0 & -\omega_x \\ -\omega_y & \omega_x & 0 \end{bmatrix}^m \begin{Bmatrix} x_P \\ y_P \\ z_P \end{Bmatrix}^m \tag{3}$$

Points P and Q are two points of the rigid reference plane that moves due to the structural deformation of the robot. If small oscillations are considered, the fixed (f) and the mobile (m) frames are nearly coincident and the rotation matrix $[R]_m^f$ is equal to the identity matrix. If a point P belongs to the Mozzi's axis, the vector product between the angular and linear velocity is equal to 0.

$$\vec{\omega} \times \left(\{ \dot{x}_p,\ \dot{y}_p,\ \dot{z}_p \}^f \right)^T = \{0\} \tag{4}$$

So, in matrix form:

$$\begin{bmatrix} 0 & -\omega_z & \omega_y \\ \omega_z & 0 & -\omega_x \\ -\omega_y & \omega_x & 0 \end{bmatrix}^f \times \left(\begin{Bmatrix} \dot{x}_Q \\ \dot{y}_Q \\ \dot{z}_Q \end{Bmatrix}^f + \begin{bmatrix} 0 & -\omega_z & \omega_y \\ \omega_z & 0 & -\omega_x \\ -\omega_y & \omega_x & 0 \end{bmatrix}^f \begin{Bmatrix} x_P \\ y_P \\ z_P \end{Bmatrix}^f \right) = \begin{Bmatrix} 0 \\ 0 \\ 0 \end{Bmatrix} \tag{5}$$

Eq. (5) are not independent, and y_P can be considered as a parameter. Hence, it is possible to write the parametric equations of the Mozzi's axis:

$$x_P = \frac{\omega_y(\omega_x \dot{x}_Q + \omega_z \dot{z}_P) - \dot{y}_P(\omega_x^2 + \omega_z^2)}{\omega_z(\omega_x^2 + \omega_y^2 + \omega_z^2)} + \frac{\omega_x z_P}{\omega_z} \tag{6}$$

$$z_P = \frac{\omega_x(\omega_y \dot{y}_P + \omega_z \dot{z}_P) - \dot{x}_P(\omega_y^2 + \omega_z^2)}{\omega_y(\omega_x^2 + \omega_y^2 + \omega_z^2)} + \frac{\omega_z y_P}{\omega_y} \tag{7}$$

Since at 79 Hz $\omega_x \approx 0$ and $\dot{y}_Q \approx 0$, the previous expressions become:

$$x_P = \frac{\omega_y \dot{z}_Q}{\omega_y^2 + \omega_z^2} \tag{8}$$

$$z_P = \frac{\omega_z}{\omega_y} y_P - \frac{\dot{x}_Q}{\omega_y} = m y_P + q \tag{9}$$

Modal tests make it possible to measure only linear accelerations of the test points (i.e. velocities and displacements, if a certain frequency is chosen). Therefore, ω_y, ω_z, $\dot{z}_Q$ and $\dot{x}_Q$ have to be calculated from measured data using the formula of rigid body motion for the 3 points ($i = 1, 2, 3$) defining the reference plane:

$$\begin{Bmatrix} \dot{x}_i \\ \dot{y}_i \\ \dot{z}_i \end{Bmatrix}^f = \begin{Bmatrix} \dot{x}_Q \\ \dot{y}_Q \\ \dot{z}_Q \end{Bmatrix}^f + \begin{bmatrix} 0 & -\omega_z & \omega_y \\ \omega_z & 0 & -\omega_x \\ -\omega_y & \omega_x & 0 \end{bmatrix}^f \begin{Bmatrix} x_i \\ y_i \\ z_i \end{Bmatrix}^f \tag{10}$$

Four equations are needed in this particular case:

$$\dot{x}_1 = \dot{x}_Q - \omega_z y_1 + \omega_y z_1 \tag{11}$$

$$\dot{x}_2 = \dot{x}_Q - \omega_z y_2 + \omega_y z_2 \tag{12}$$

$$\dot{x}_3 = \dot{x}_Q - \omega_z y_3 + \omega_y z_3 \tag{13}$$

$$\dot{z}_1 = \dot{z}_Q - \omega_y x_1 \tag{14}$$

From the first three equations ω_z, ω_y and $\dot{x}_Q$ can be calculated solving a linear system. Then, independently, velocity $\dot{z}_Q$ can be calculated from Eq. (14).

5 Identification of link compliance

The definition of the group of 3 points on the "rigid part" of the robot is somewhat arbitrary. Using Equations 8 and 9, the slope m, the intercept q and the coordinate x_P of the Mozzi's axis can be computed for different combinations of 3 points. For different groups of points, the Mozzi's axis should be the same if the considered part of the robot moves as a rigid body. In this case, 6 different sets of points are considered. In Table 5 the slope m, the intercept q and the coordinate x_p of the identified Mozzi's axes are reported. The Mozzi's axes are shown in Figure 5.

Table 5. Slope m, intercept q and the coordinate x_p of each considered plane.

Points	*14 15 16*	*13 15 16*	*12 14 16*	*11 15 16*	*11 14 15*	*11 14 16*
m [/]	-0.31	-0.26	-0.33	-0.28	-0.28	-0.29
q [mm]	187.2	217.6	193.8	203.9	191.9	178.6
x_P [mm]	17.0	26.0	12.6	21.6	17.5	14.6

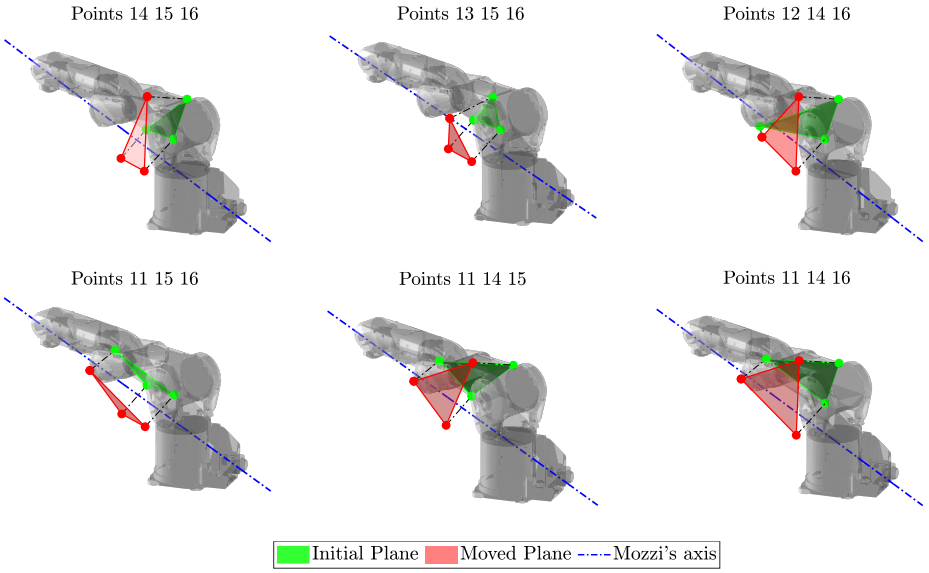

Fig. 5. Mozzi's axis considering different groups of points.

The position of the Mozzi's axis is only slightly different if different groups of points are considered. This result corroborates the assumption that at 79 Hz the links after joint 1 essentially behave as a rigid body. Finally, the average Mozzi's axis, which is the compliance axis of the robot, is calculated. The average slope is $\bar{m} = -0.29$, the average intercept is $\bar{q} = 195.5\ mm$ and the average X-coordinate is $\bar{x}_P = 18.2\ mm$. Figure 6 shows that the Mozzi's axis, as previously hypothesized, passes through link 1 and near points 3 and 4 that are located on link 5. This location of the compliance axis explains why the X displacements of points 1 and 2 (which are below the compliance axis) are in phase opposition with respect to the displacements of the other points. From the position of the compliance axis, it is possible to evaluate the inertia of the system about this axis by means of the CAD model. Finally, using Eq. (1) it is possible to evaluate the structural stiffness about the compliance axis.

With $I_{zz_7} = 0.55\ Kg\ m^2$, and $f_{n_i} = 79\ Hz$ structural stiffness is: $k_7 = 135511\ Nm/rad$, Eq. (2) with the same f_{n_i} gives $c_7 = 14.2\ Nms/rad$. It is worth noticing that the link stiffness is much larger than the identified joint stiffness values.

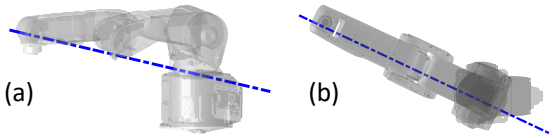

Fig. 6. Average Mozzi's axis. (a) Axonometric view. (b) Upper view.

6 Conclusions

The application of the Mozzi's axis concept has made possible the identification of the compliance axis of the robot related to the measured resonance peak at 79 Hz. Therefore, the vibrational behavior of the robot can be simulated considering the first 3 actual joints equipped with the identified joint stiffness and a virtual joint aligned to the identified compliance axis and with rotation stiffness equal to the identified value. The proposed method can be used for finding the compliance characteristics of other serial robots if at a certain frequency the compliance is due to a specific link or bearing, while the other robot's components behave as rigid bodies. The analysis of complex cases (e.g. modes involving both structural and joints compliance) may require a different approach.

7 References

1. Pan, Z. *et al.*.: Chatter analysis of robotic machining process. Journal of materials processing technology, 173(3), 301-309, (2006)
2. Carbone, G.: Stiffness analysis and experimental validation of robotic systems. Frontiers of Mechanical Engineering, 6(2), 182-196, (2011)
3. Zhou, J. *et al.*.: A hybrid least-squares genetic algorithm–based algorithm for simultaneous identification of geometric and compliance errors in industrial robots. Advances in Mechanical Engineering, 7(6), 1687814015590289, (2015)
4. Zhou, J. *et al.*.: Simultaneous identification of joint compliance and kinematic parameters of industrial robots. International journal of precision engineering and manufacturing, 15(11), 2257-2264, (2014)
5. Boby, R. A.: Identification of elasto-static parameters of an industrial robot using monocular camera. Robotics and Computer-Integrated Manufacturing, 74, 102276, (2022)
6. Gonzalez, M. K. *et al.*.: Online compliance error compensation system for industrial manipulators in contact applications. Robotics and Computer-Integrated Manufacturing, 76, 102305, (2022)
7. Bottin, M. *et al.*.: Modeling and identification of an industrial robot with a selective modal approach. Applied Sciences, 10(13), 4619, (2020)
8. Doria, A. *et al.*.: The twist axis of frames with particular application to motorcycles. Proceedings of the institution of mechanical engineers, part C: Journal of mechanical engineering science, 230(17), 3026-3039, (2016)
9. Doria, A. *et al.*.: Analysis of the compliance properties of an industrial robot with the Mozzi axis approach. Robotics, 8(3), 80, (2019)
10. Siciliano, B. *et al.*.: Robotics: modelling, planning and control. Springer Science & Business Media (2010)